ST3GAL1 Promotes Malignant Phenotypes in Intrahepatic Cholangiocarcinoma

Authors

Fanghua Chen, Ke Gao, Yan Li, Yin Li, Yingcheng Wu, Liangqing Dong, Zijian Yang, Jieyi Shi, Kun Guo, Qiang Gao, Haojie Lu, and Shu Zhang

Correspondence

luhaojie@fudan.edu.cn; zhang.shu@zs-hospital.sh.cn

Graphical Abstract

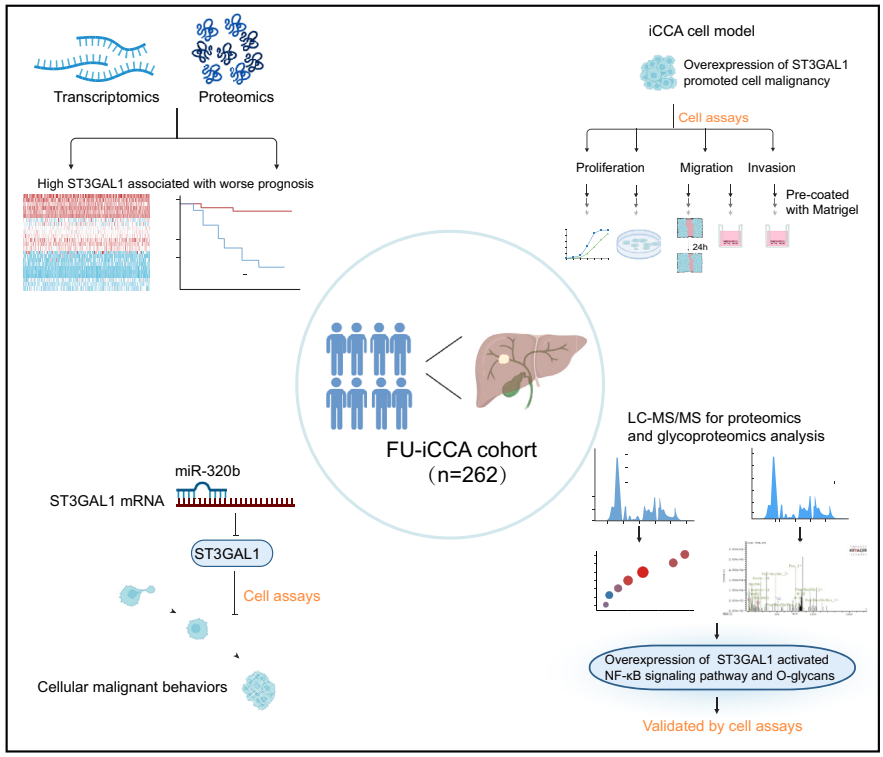

In Brief

Chen *et al*. identify ST3GAL1 as a prognostically relevant molecule in intrahepatic cholangiocarcinoma (iCCA). The study suggests ST3GAL1, regulated by miR-320b, promotes iCCA cell malignancy through the NF-κB signaling pathway. Notably, glycoproteomics show O-glycosylation is changed in iCCA cells with high ST3GAL1 expression and differential O-glycopeptides underscoring the potential utility of O-glycosylation profiling as a discriminatory marker for ST3GAL1-overexpressing iCCA cells. These results suggest that ST3GAL1 could serve as a promising therapeutic target for iCCA.

Highlights

- ST3GAL1 is identified as a prognostically relevant molecule in iCCA.
- miR-320b regulates ST3GAL1, promotes iCCA cell malignancy *via* NF-κB pathway.
- ST3GAL1-mediated O-glycosylation changes may serve as a marker for iCCA cells.

2024, Mol Cell Proteomics *23*(*9*), 100821

https://doi.org/10.1016/j.mcpro.2024.100821

ST3GAL1 Promotes Malignant Phenotypes in Intrahepatic Cholangiocarcinoma

Fanghua Chen[1,‡], Ke Gao[1,‡], Yan Li[1], Yin Li[2], Yingcheng Wu[1], Liangqing Dong[1], Zijian Yang[1], Jieyi Shi[1], Kun Guo[1], Qiang Gao[1], Haojie Lu[1,3,*], and Shu Zhang[1,*]

Intrahepatic cholangiocarcinoma (iCCA) has a poor prognosis, and elucidation of the molecular mechanisms underlying iCCA malignancy is of great significance. Glycosylation, an important post-translational modification, is closely associated with tumor progression. Altered glycosylation, including aberrant sialylation resulting from abnormal expression of sialyltransferases (STs) and neuraminidases (NEUs), is a significant feature of cancer cells. However, there is limited information on the roles of STs and NEUs in iCCA malignancy. Here, utilizing our proteogenomic resources from a cohort of 262 patients with iCCA, we identified ST3GAL1 as a prognostically relevant molecule in iCCA. Moreover, overexpression of ST3GAL1 promoted proliferation, migration, and invasion and inhibited apoptosis of iCCA cells *in vitro*. Through proteomic analyses, we identified the downstream pathway potentially regulated by ST3GAL1, which was the NF-κB signaling pathway, and further demonstrated that this pathway was positively correlated with malignancy in iCCA cells. Notably, glycoproteomics showed that O-glycosylation was changed in iCCA cells with high ST3GAL1 expression. Importantly, the altered O-glycopeptides underscored the potential utility of O-glycosylation profiling as a discriminatory marker for iCCA cells with ST3GAL1 overexpression. Additionally, miR-320b was identified as a post-transcriptional regulator of ST3GAL1, capable of suppressing ST3GAL1 expression and then reducing the proliferation, migration, and invasion abilities of iCCA cell lines. Taken together, these results suggest ST3GAL1 could serve as a promising therapeutic target for iCCA.

Intrahepatic cholangiocarcinoma (iCCA) is a highly malignant bile duct cancer that accounts for 5% to 10% of primary liver malignancies, making it the second most common type of liver cancer (1). Unfortunately, the majority of individuals with iCCA are diagnosed at an advanced stage, and conventional radiation and chemotherapy treatments have demonstrated limited efficacy in enhancing long-term survival rates (2). Roughly 20%-30% of patients are suitable for resection, which is considered the sole potentially curative treatment. Following resection, a median survival of 53 months has been reported when combined with adjuvant capecitabine. However, for 70%-80% of patients presenting with locally unresectable or distant metastatic disease, systemic therapy may postpone progression, yet survival is still confined to approximately 1 year (3). Moreover, the lack of understanding of the molecular mechanisms driving iCCA growth hampers the development of new therapies. Therefore, it is imperative to investigate the molecular pathogenesis of iCCA to pave the way for new therapeutic approaches.

Abnormal glycosylation is a hallmark of cancer and plays a significant role in tumor initiation, development, and metastasis (4). Changes in glycosylation patterns, including alterations in sialylation, fucosylation, GlcNAc-branching of N-glycans, and truncated O-glycans have been observed in cancers (5, 6). These aberrant glycans are functionally involved in key events related to cancer progression, such as inflammation, angiogenesis, invasion, and metastasis (7, 8). Investigating the abnormal glycosylation patterns, regulated by glycosyltransferases or glycosidases, is essential for understanding the mechanisms underlying iCCA progression and metastasis.

Sialylation is a biologically important modification that is related to embryonic development, neurodevelopment, reprogramming, oncogenesis, and immune response (9). Sialic acid is transferred to glycolipids and glycoproteins by different sialyltransferases (STs), which include 20 conserved enzymes further divided into four subfamilies: ST3GAL, ST6GAL, ST6GalNAc, and ST8SIA (10). Among these, ST3GAL1 adds a sialic acid in an α2,3 linkage to Gal β1,3 GalNAc and its overexpression leads to an increase in the sialylation of O-glycan Tn to Sialyl-Tn in cancer (11). Moreover, change in O-glycosylation is one of the most prevalent glycotypes observed in solid tumors (5) and often results in O-glycoproteins carrying short, linear sialylated glycans rather than the longer branched glycans seen in normal epithelial cells (12).

From the [1]Liver Cancer Institute, Zhongshan Hospital, Key Laboratory of Carcinogenesis and Cancer Invasion (Ministry of Education), [2]Department of Thoracic Surgery, Zhongshan Hospital, and [3]Department of Chemistry and NHC Key Laboratory of Glycoconjugates Research, Institutes of Biomedical Sciences, Fudan University, Shanghai, China

‡These authors contributed equally to this work.

*For correspondence: Haojie Lu, luhaojie@fudan.edu.cn; Shu Zhang, zhang.shu@zs-hospital.sh.cn.

https://doi.org/10.1016/j.mcpro.2024.100821

On the contrary, neuraminidases (NEUs), including NEU1, NEU2, NEU3, and NEU4, remove sialic acid in cells and are associated with cell-cell adhesion, migration, and proliferation (13). However, the associations of STs or NEU levels with clinical significance in patients with iCCA are not well-studied.

MicroRNAs (miRNAs) are small non-coding RNA molecules that play a crucial role in post-transcriptional gene regulation. They are important modifiers of protein expression, interacting with the 3′-untranslated region (3′-UTR) of mRNA to regulate expression levels (14). Glycosylation is regulated by a complex network of biosynthetic enzymes at various levels (15). The miRNAs have been established as major regulators of glycosylation (16, 17), and their role in controlling STs or NEUs levels was studied to a limited extent.

In this study, we utilized proteogenomic resources from a cohort of 262 patients with iCCA (18) to investigate the impact of STs and NEUs on the prognosis of iCCA. Our results revealed a significant association between ST3GAL1 and iCCA prognosis. Subsequently, we explored the biological function of ST3GAL1 and its impact on iCCA cell functions, as well as seeking potential mechanisms by employing proteomic and glycoproteomic strategies. Our findings demonstrated that overexpression of ST3GAL1 promoted tumor proliferation, migration, and invasion, while simultaneously inhibiting cell apoptosis through the NF-κB signaling pathway *in vitro. Additionally, ST3GAL1 was found to play a role in modulating the O-glycosylation levels of iCCA cells*. The overexpression of ST3GAL1 contributed to alterations in O-glycopeptide abundances. We further identified miR-320b as a regulator of ST3GAL1, which not only inhibited ST3GAL1 expression but also suppressed malignancy in iCCA cells.

MATERIALS AND METHODS

Patients and iCCA Biopsy Specimens

The iCCA samples utilized in this study were described in a previous study (18). The tissue samples were obtained from patients who had previously undergone surgery at Zhongshan Hospital. Briefly, once the tissues were obtained, they were placed in a 50 ml centrifuge tube containing cell culture medium and placed in an ice box for immediate transportation to the laboratory (within 2 h). After washing with cold PBS and wiping dry with absorbent paper, then approximately 1 cm × 1 cm × 0.5 cm tissues were soaked in 4% paraformaldehyde. Other tumor tissues were frozen with liquid nitrogen and stored in a −80 °C degree freezer until further analysis. The study received approval from the Research Ethics Committee of Zhongshan Hospital (B2021–075R). All human studies reported in this study were conducted in accordance with the Declaration of Helsinki.

Tissue Microarray and Immunohistochemistry

TMA comprising 196 tumor tissues from patients with iCCA having comprehensive prognostic information was assembled previously (18). Immunohistochemistry was performed according to our previous study (19). Briefly, tumor tissue slides were rehydrated, antigen retrieved, blocked, and then incubated with ST3GAL1 monoclonal antibody (1:1000, Catalog#ab96129, Abcam). After 12 h, the slides were treated with secondary antibodies and subjected to color development using the DAB peroxidase substrate kit (Catalog#P0202, Beyotime). The staining levels were assessed by two independent pathologists. To assess ST3GAL1 staining, a staining index was utilized by combining the score for the percentage of positive tumor cells with the intensity score. The percentage of positive cells was categorized as follows: 0 (<10%), 1 (10–25%), 2 (26–50%), 3 (51–75%), and 4 (76–100%). Additionally, the intensity of staining was scored as 0 (negative), 1 (weak), 2 (medium), or 3 (strong). Sections with a final score of less than four were classified as having low ST3GAL1 expression.

Cell Culture

The cell lines (RBE, HuCC-T1, HCCC-9810, 293T) were acquired from the Liver Cancer Institute of Zhongshan Hospital (Shanghai, China) and cultured in Roswell Park Memorial Institute (RPMI) 1640 medium (Catalog#11875119, Gibco). All mediums were supplemented with 10% fetal bovine serum (FBS, Catalog#12483012, Gibco) and 1% Penicillin-streptomycin (Catalog#15140163, Gibco). The 293T cells were cultured in DMEM supplemented with 10% FBS and 1% Penicillin-streptomycin. All cells were incubated in a humidified incubator at 37 °C with 5% CO_2. Short tandem repeat analyses were performed on these cell lines to ensure their authentication.

Lentivirus Infection and Oligonucleotide Transfection

The vectors of pLKO.1-Puromycin-shRNA-ST3GAL1, pLKO.1-Puromycin-NC, and pLVX-Puromycin-ST3GAL1 were obtained from Ruoji Technology (Shanghai, China) and were transfected into HuCC-T1 and HCCC-9810 cells. Three short-hairpin RNA (shRNA) target sequences were mixed with the same proportion. The iCCA cells were infected with lentivirus using polybrene (5 μg/ml) and subsequently selected with puromycin (2 μg/ml) for 7 days. During this selection process, individual cells that did not integrate the lentiviral construct or did not express the target gene were eliminated, while the successfully modified cells continued to proliferate, leading to the establishment of clonally selected stable ST3GAL1-silencing (HuCC-T1 KD) or ST3GAL1-overexpressing cell lines (HCCC-9810 OE).

The miR-320b mimics, inhibitor, and negative control were obtained from Genomeditech. The cells were seeded in a six-well plate until 70% confluence and then transfected with the miRNA mimics, inhibitor, or negative control using Lipofectamine 2000 (Catalog#11668030, Invitrogen) according to the instructions of the manufacturer. After 48 h, the above-mentioned cells were used for function experiments. Western blot and qRT-PCR were performed to evaluate the ST3GAL1 expression. The sequences of ST3GAL1, sh-ST3GAL1, miR-320b mimics, inhibitor, and negative control have been shown in Supplemental Table S1.

RNA Isolation, Reverse Transcription, and qRT-PCR Analysis

Total RNA was extracted using Trizol reagent (Catalog#15596026, Invitrogen). Subsequently, reverse transcription was conducted using the first-strand cDNA synthesis supermix (Catalog#11141ES60, YEASEN). For quantitative real-time PCR analysis, the Step One Plus Real-Time PCR System was employed along with qPCR SYBR green mix (Catalog#11203ES08, YEASEN). The mRNA level of GAPDH was employed as a control to quantify the relative expression of ST3GAL1. Relative transcript levels were analyzed using the cycling threshold ($2^{-\Delta\Delta Ct}$) method. Samples from each experiment were analyzed in triplicate.

Western Blotting

Western blot analysis was performed according to our previous study (19). The antibodies utilized in this study were listed as follows: ST3GAL1 (1:1000, ab96129, Abcam); β-Tubulin (1:1000, 2146, CST);

P65 (1:1000, 8242, CST); p-P65 (1:1000, 3033, CST); IκBα (1:1000, 4814, CST); p-IκBα (1:1000, 9246, CST); HRP-conjugated secondary antibodies (1:7500, AB-10015289&AB-2313567, Jackson Immunoresearch).

Lectin Blot Analysis

The equivalent whole-cell protein solution was separated using 10% SDS-PAGE, transferred onto PVDF membranes, and blocked with blocking buffer. The membranes were then probed with biotinylated lectins at room temperature for 30 min as follows: *Maackia amurensis* lectin I (MAL-I, 2 μg/ml, Catalog#B1315, Vector), and *Maackia amurensis* lectin II (MAL-II, 5 μg/ml, Catalog#B-1265, Vector). Afterward, they were incubated with biotin-labeled horseradish peroxidase (Catalog#A0308, Beyotime) for another 30 min. Blots were imaged *via* ECL detection. Following the testing, the PVDF membrane was incubated in a solution of primary antibody and secondary antibody removal (Catalog#P0025, Beyotime) for 20 min. Subsequently, it was rinsed three times for 5 min each with TBS-T buffer and incubated with β-Tubulin for a new round of detection.

Cell Counting Kit-8 and Colony Formation Assay

Cells were seeded at a density of 3000 cells/well in 96-well plates. Cell viability was assessed every 24 h for 5 days using the Cell counting kit-8 (CCK-8, Catalog#C0038, Beyotime), following the manufacturer's instructions.

In the colony formation assay, cells were seeded in six-well plates at a density of 1000 cells/well and cultured in complete RPMI 1640 medium for 2 weeks. Afterward, the colonies were fixed in 4% paraformaldehyde for 30 min and stained with crystal violet staining solution (Catalog#C0121, Beyotime). Images were captured, and the colonies were counted using Image J software.

Flow Cytometry Assay

Cells were digested using 0.25% trypsin and subsequently washed twice with PBS. They were then adjusted to a concentration of 5×10^5 cells. Next, a mixture of 5 μl of Annexin V-FITC and 10 μl of propidium staining solution (Catalog#40302ES20, YEASEN) was added to 100 μl of 1× binding buffer and incubated at room temperature for 15 min in the dark. Following this, 400 μl of 1× binding buffer was added. Flow cytometry (FACSVantageSE, BD, USA) was utilized to detect apoptosis.

Migration and Invasion Assays

The migration and invasion assays were conducted using Boyden chambers with an 8 μm pore size (Catalog#351152, Corning). Cells were suspended in a serum-free medium, and RPMI 1640 medium supplemented with 10% serum served as the chemoattractant. Following suitable incubation time, migrated cells were fixed in 4% paraformaldehyde for 30 min and stained with crystal violet staining solution for 1 h. Cell counts were performed in three different fields using a Leica DMI3000 B microscope.

For the invasion assay, each chamber was pre-coated with 100 μl of Matrigel (diluted 1:8 with RPMI 1640 medium) at 37 °C for 4 h. Cells were suspended in serum-free medium and added onto the Matrigel coating, while RPMI 1640 medium supplemented with 10% serum was used as the chemoattractant. After appropriate incubation, non-invading cells were removed, and the remaining cells were fixed, stained, and counted. Results were obtained from three independent experiments.

Wound-Healing Assay

Cells were cultured in 6-well plates with RPMI 1640 medium until they formed a confluent monolayer covering the entire bottom of the plate. A scratch was created on the cell monolayer using a sterile 200 μl pipette tip, after which the cells were further cultured in RPMI 1640 medium without FBS for an additional 24 h. Migrated cells within the scratch area were counted in three randomly selected fields using a light microscope. The scratch areas were measured using Image J software.

Transcriptome Analysis

Total RNA was extracted from iCCA cells following the manufacturer's protocol using TRIzol Reagent. Subsequently, mRNAseq libraries were constructed from the total RNA using the Illumina TruSeq mRNA sample preparation kit and sequenced on an Illumina HiSeq 2500 platform with a 2 × 50 bp setup. The assembled transcripts were then compared against the National Center for Biotechnology Information (NCBI) database. Gene expression levels were quantified using Htseq software (V0.6.1), which employs the FPKM (Fragments Per Kilobase per Million reads) method for calculating gene expression (20). The FPKM values of genes in the transcriptome of iCCA cells can be accessed in Supplemental Table S2.

Preparation of Peptides

Cell protein concentrations were determined using the BCA assay. A total of 500 μg of proteins were first reduced with 10 mM dithiothreitol (DTT) at 55 °C for 30 min and subsequently alkylated with 20 mM iodoacetamide (IAA) at RT for 30 min in the dark. The proteins were then digested with sequencing grade modified trypsin (Promega, 50:1, w/w) at 37 °C overnight with shaking. To quench the reaction, trifluoroacetic acid (TFA) was added to a final concentration of 0.1% (v/v). The digested samples were desalted using C18 Sep-Pak cartridges (Waters). The resulting tryptic digestions of the proteins were then lyophilized and stored.

For O-glycopeptides, 2 μl PNGase F (Catalog#P0704S, New England Biolabs) was added to the trypsin-digested samples and made a 20 μl total reaction volume, reacted at 37 °C overnight to remove most of the N-glycans according to the manufacturer's instructions. The samples were desalted by using C18 Sep-Pak cartridges.

Glycopeptide Enrichment

O-glycopeptides were enriched using homemade ZIC-HILIC (Merck, 5 μm, 200 Å) SPE column. The ZIC-HILIC packings were pre-equilibrated with the washing buffer (80% acetonitrile (ACN), 5% TFA). The desalted peptide solution was loaded onto the column, and after washing, the O-glycopeptides were sequentially eluted with 400 μl of 50 mM ammonium bicarbonate and 400 μl of 0.1% TFA. The eluants were combined, dried in a SpeedVac, and resuspended in 100 μl of 0.1% TFA.

Nano-HPLC-MS/MS for Proteomic Analysis

The peptides were resuspended in 7 μl of solvent A (A: water with 0.1% formic acid (FA); B: 80% ACN with 0.1% FA), separated by nanoLC, and analyzed using online electrospray tandem mass spectrometry. The experiments were conducted on an EASY-nLC 1200 UPLC system connected to an Orbitrap Exploris 480 mass spectrometer (Thermo Fisher Scientific) with an online nano-electrospray ion source. A 5 μl peptide sample was loaded onto a trap column (Thermo Scientific Acclaim PepMap C18, 100 μm × 2 cm) at 10 μl/min for 3 min, then separated on an analytical column (Acclaim PepMap C18, 75 μm × 50 cm) with a linear gradient from 5% B to 40% B over 105 min, followed by a 9 min increase from 40% to 50% B and a 1 min climb to 100% B, held at 100% for 5 min. The column was re-equilibrated for 10 min and maintained at a flow rate of 300 nl/min and column temperature of 60 °C.

The Orbitrap Exploris 480 mass spectrometer operated in data-dependent mode, switching automatically between MS and MS/MS

acquisition. Full-scan MS spectra (m/z 350–1600) were acquired with a mass resolution of 60K. The automatic gain control (AGC) target was set to 3,000,000, maximum injection time (IT) of 50 ms for MS scans, and 75,000 AGC target, intensity threshold of 20,000, and a maximum IT of 25 ms for MS/MS. One microscan was recorded using 30 s dynamic exclusion. HCD fragmentation was automatically selected for precursor ions with charge states 2 to 5+ and intensity above 20,000. Precursors were fragmented in the orbitrap at a normalized collision energy of 30% for a cycle time of 2 s, with a fixed first mass of 110.

Nano-HPLC-MS/MS for Glycoproteomic Analysis

The peptides were resuspended with 7 μl solvent A respectively (A: water with 0.1% FA; B: 80% ACN with 0.1% FA), separated by nanoLC and analyzed by online electrospray tandem mass spectrometry. The experiments were performed on EASY-nLC 1200 UPLC system connected to Orbitrap Exploris 480 mass spectrometer (Thermo Fisher Scientific) equipped with an online nano-electrospray ion source. The 5 μl peptide sample was loaded onto the trap column (Thermo Scientific Acclaim PepMap C18, 100 μm × 2 cm), with a flow of 10 μl/min for 3 min and subsequently separated on the analytical column (Acclaim PepMap C18, 75 μm × 50 cm) with a linear gradient, from 2% B to 35% B over 75 min, 35% to 55% in 9 min and climbing to 100% in 1 min then holding at 100% for the last 5 min. The column was re-equilibrated at initial conditions for 10 min. The column flow rate was maintained at 300 nl/min and the column temperature was maintained at 60 °C. The electrospray voltage of 2.3 kV *versus* the inlet of the mass spectrometer was used.

The Orbitrap Exploris 480 mass spectrometer was operated in the data-dependent mode to switch automatically between MS and MS/MS acquisition. Survey full-scan MS spectra (m/z 350–1600) were acquired with a mass resolution of 120K. For MS scans, the AGC target was set to 3,000,000, and the maximum injection time was 50 ms. For MS/MS, the intensity threshold was 20,000, the maximum injection time was 50 ms and the AGC target was set to 100,000. In all cases, one microscan was recorded using dynamic exclusion of 30 s. MS/MS fixed first mass was set at 110 and the normalized collision energy of HCD was set to 30%. Precursor ions with a charge state 2 to 5+ and an intensity above 20,000 were automatically selected for HCD fragmentation in the orbitrap for a cycle time of 2 s.

Data Processing and Bioinformatic Analysis

All of the raw files were searched and compared against the UniProt human protein sequence database (Jan 2022 containing 20,376 reviewed protein sequences). The protein quantification was performed using Proteome Discoverer software (Thermo Fisher Scientific, version 3.0.0.757), and Abundances (normalized) was chosen. The glycopeptide quantification was performed using Byologic (Protein Metrics Inc.). With Byologic, the peak area of the extracted-ion chromatogram (XIC) of a given glycopeptide was automatically integrated. We have compiled the parameters for Nano-HPLC-MS/MS used in proteomic and glycoproteomic analyses and presented them in Supplemental Table S3.

Tandem mass spectra were extracted using Proteome Discoverer software (Thermo Fisher Scientific, version 3.0.0.757) and searched against the human protein database with the assumption of trypsin digestion. The input parameters were: 10 ppm precursor mass tolerance and 0.02 Da fragment mass tolerance. The fixed modification was carbamidomethylation on all Cys residues (C + 57.022 Da). Variable modifications included oxidation on Met (M + 15.995 Da) and acetylation on protein N-term (+42.011 Da). Maximum missing cleavage locations were limited to two. The maximum false discovery rates (FDR) for protein and peptides were set at 1%. Proteins identified in iCCA cell lines based on quantitative proteomics were listed in Supplemental Table S4.

O-glycopeptide identification was performed using Byonic version 3.7.13, and quantification was performed by Byologic version 3.7 (21). The identified glycopeptides from the Byonic (screening Score ≥200 & |Log Probability| ≥ 2 as the cutoff value, with repeat glycopeptides removed) were chosen. All the identified data can be obtained at iProx with project ID IPX0007264000. Byologic utilizes Byonic search results as inputs to compute the XICs and relative abundances *via* a default label-free quantification approach within the Byologic software. Quantification of O-glycopeptides in iCCA cells using Byologic was listed in Supplemental Table S5.

O-glycan compositions were obtained based on the number of each type of residue, HexNAc(a)Hex(b)Fuc(c)NeuAc(d), where a refers to the number of N-acetylhexosamine, b referred to the number of hexose, c referred to the number of fucoses, and d refers to the number of N-acetylneuraminic acid. HexNAc(a)Hex(b)NeuAc(d) was classified as sialylated glycan when d ≥ 1. Examples of O-glycopeptide tandem MS spectra have been shown in Supplemental Fig. S1.

Pathway Analysis

Pathway analysis was used to explore the significant pathways of the deferentially expressed proteins (DEPs) analysis based on the Kyoto Encyclopedia of Genes and Genomes (KEGG) database. In DEPs analysis, we eliminated proteins, which only showed once in three analytic MS runs, and *t* test analysis was performed to find DEPs with $p < 0.05$ and the absolute value of $\log_2(|FC|) > 1$. The Fisher exact test was used to identify significant pathways, and the threshold of significance was defined using the *p* value and FDR.

Statistical Rationale

Three biological replicates were carried out for label-free quantitative proteomic analysis. Proteins identified in three replicates with 'peptides' ≥1 and 'unique peptides' >1, and 1% FDR at peptide and protein levels for each cell line were considered. In glycoproteomic experiments, O-glycopeptides quantified at least in duplicate in both HCCC-9810 OE and Vector cells were applied for differential glycopeptide analysis (22).

Statistical analysis was performed using GraphPad Prism (version 8.0, GraphPad Software, Inc.), Excel, and Hiplot (https://hiplot.org), which were also used for data processing and presentation. Differentially expressed proteins in HCCC-9810 OE versus HCCC-9810 Vector or HuCC-T1 KD versus HuCC-T1 NC were identified by using paired two-tailed Student's *t* test with a threshold of $\log_2$(|fold change|) > 1, for example, $\log_2$(|fold change (HCCC-9810 OE)/(HCCC-9810 Vector)|) > 1 or $\log_2$(|fold change (HuCC-T1 KD)/(HuCC-T1 NC)|) > 1). Moreover, following the normalization of O-glycopeptide abundance by the corresponding protein abundance, the fold change for the normalized O-glycopeptide abundance was calculated as the ratio between HCCC-9810 OE and Vector. A significance threshold of $\log_2$(|fold change|) > 1 and $p < 0.05$ was applied to identify significant changes in normalized O-glycopeptides.

When scoring the intensity of immunohistochemical staining, the researchers were blinded. Student's *t* test was used for two groups of comparisons and rank-sum test was used for multiple comparisons. Kaplan-Meier analyses were used for survival analysis. The independent prognostic factor was investigated by using the Cox proportional hazards regression model.

RESULTS

Clinical Importance of ST3GAL1 in iCCA

To gain insights into the role of STs and NEUs in conferring clinical response to iCCA, we analyzed the gene and protein expression of STs and NEUs from a cohort of 262 patients

with iCCA (18). The analysis revealed that ST6GAL1 and ST3GAL1 were highly expressed in iCCA (Supplemental Fig. S2*A*) and a strong correlation between mRNA and protein levels for ST6GAL1 and ST3GAL1 (Supplemental Fig. S2*B*). In an effort to bridge the gap between clinical specimens and cell lines, we presented comprehensive information on the transcriptomic profiles of sialyltransferases and neuraminidases in three iCCA cell lines. Transcriptomic analysis showed that ST3GAL1 level was high in three iCCA cells, however, ST6GAL1 was decreased significantly in HCCC-9810 (Supplemental Fig. S2*C*). Then, we focused on ST3GAL1 for further investigation. We then assessed the clinical significance of ST3GAL1 expression in patients with iCCA . Kaplan-Meier survival analysis, utilizing data from 214 patients with prognostic information, revealed that individuals exhibiting high ST3GAL1 expression had significantly lower progression-free survival (PFS) and overall survival (OS) rates compared to those with weaker ST3GAL1 expression (Fig. 1, *A* and *B*). Additionally, serum carcinoembryonic antigen (CEA) and carbohydrate antigen 19-9 (CA19–9) exhibited low diagnostic sensitivity; however, their simultaneous elevation was linked to a higher risk of presenting with locally advanced or metastatic iCCA (23). Furthermore, we observed a positive correlation between CEA and CA19-9 levels in iCCA, and ST3GAL1 was also positively correlated with the CEA and CA19-9, respectively (Fig. 1*C*). To further validate the clinical significance of high ST3GAL1 expression in iCCA, we utilized tissue microarrays to detect ST3GAL1 expression in patients with iCCA (Fig. 1, *D* and *E*). Then, cox regression analysis was employed and the result also revealed that increased ST3GAL1 level was an independent prognostic factor for patients with iCCA and has a good synergistic prognostic value with clinical biomarkers including CEA and CA19-9 (Table 1). These findings suggested that ST3GAL1 might play certain roles in the progression of iCCA and its potential functions were explored in the following studies.

Overexpression of ST3GAL1 Promoted iCCA Cell Proliferation and Suppressed Cell Apoptosis

We extended our investigation by utilizing the iCCA cell line to explore the biological function of ST3GAL1. The endogenous expression of ST3GAL1 in iCCA cells (HuCC-T1, HCCC-9810, RBE) was assessed through ELISA and Western blot and the result showed HuCC-T1 had the highest endogenous ST3GAL1 expression while HCCC-9810 had the relative lower endogenous levels (Fig. 2*A* and Supplemental Fig. S2*D*). To investigate the biological functions of ST3GAL1, HCCC-9810 cells were stably transduced with either an empty lentiviral vector (Vector) or an ST3GAL1 overexpression (OE) vector, while HuCC-T1 cells were transduced with a ST3GAL1-targeting shRNA construct to knockdown (KD) expression of ST3GAL1. After transfection, we validated the efficacy of overexpression and knockdown at the transcriptional level using real-time PCR (Fig. 2*B*), and at the protein level using ELISA and Western blot (Fig. 2*C* and Supplemental Fig. S2*E*). The proliferation ability of stable iCCA cell lines was subsequently measured and the results showed that the proliferation ability was increased in HCCC-9810 OE cells, while HuCC-T1 KD cells had a decreased proliferation ability compared to that in negative control (NC) cells (Fig. 2*D*). Cell apoptosis was assessed using flow cytometry assay, which revealed an elevated number of apoptotic cells in HuCC-T1 KD cells compared to HuCC-T1 NC cells, and a reduced number of apoptotic cells in HCCC-9810 OE cells compared to HCCC-9810 Vector cells (Fig. 2*E*).

High ST3GAL1 Levels Increased the Proliferation, Invasion, and Migration of iCCA Cells

Furthermore, the potential role of ST3GAL1 in colony formation, migration, and invasion of iCCA cells was measured *in vitro*. As illustrated in Figure 3*A*, overexpression of ST3GAL1 significantly increased the colony number in HCCC-9810 cells, whereas knockdown of ST3GAL1 led to a reduction in colony numbers in HuCC-T1 cells. Meanwhile, Matrigel-coated Transwell assays revealed enhanced invasive abilities of HCCC-9810 OE cells, whereas HuCC-T1 KD cells exhibited reduced invasive capacity (Fig. 3*B*). Matrigel-free Transwell and wound healing assays demonstrated that overexpression of ST3GAL1 promoted the migration of HCCC-9810 cells, whereas silencing ST3GAL1 had the opposite effect on HuCC-T1 cells (Fig. 3, *C* and *D*). These findings provided evidence of the involvement of ST3GAL1 in promoting the malignant behaviors of iCCA cells.

ST3GAL1 was Associated with NF-κB Signaling Pathway in iCCA Cells

We next assessed the mechanism of ST3GAL1 in promoting iCCA malignant behaviors by performing proteomics. The proteomic analysis showed significant enrichment of high ST3GAL1 expression related to several classical pathways, particularly the NF-κB signaling pathway (Fig. 4*A*). Therefore, we proposed that ST3GAL1 might promote iCCA cell malignant behaviors by regulating the NF-κB signaling pathway. Due to the typical indication of NF-κB signaling pathway activation with increased p-P65 and p-IκBα levels (24), we conducted Western blot analysis to detect the expression of NF-κB signaling pathway-related proteins (P65, p-P65, IκBα, and p-IκBα). The results showed that p-IκBα and p-P65 proteins were downregulated in HuCC-T1 KD cells, while upregulated in HCCC-9810 OE cells (Fig. 4*B*). Additionally, treatment with caffeic acid phenethyl ester (CAPE, 30 μM/ml), an inhibitor of the NF-κB pathway (25), reversed the effects of ST3GAL1 overexpression on the activation of the NF-κB pathway (Supplemental Fig. S3*A*). Adding CAPE (30 μM/ml) into HuCC-T1 WT and HCCC-9810 OE cells also reversed the overexpression of ST3GAL1 mediated in cell proliferation (Supplemental Fig. S3*B*), colony number (Fig. 4*C*), apoptosis (Fig. 4*D*), invasion (Supplemental Fig. S3*C*) and migration

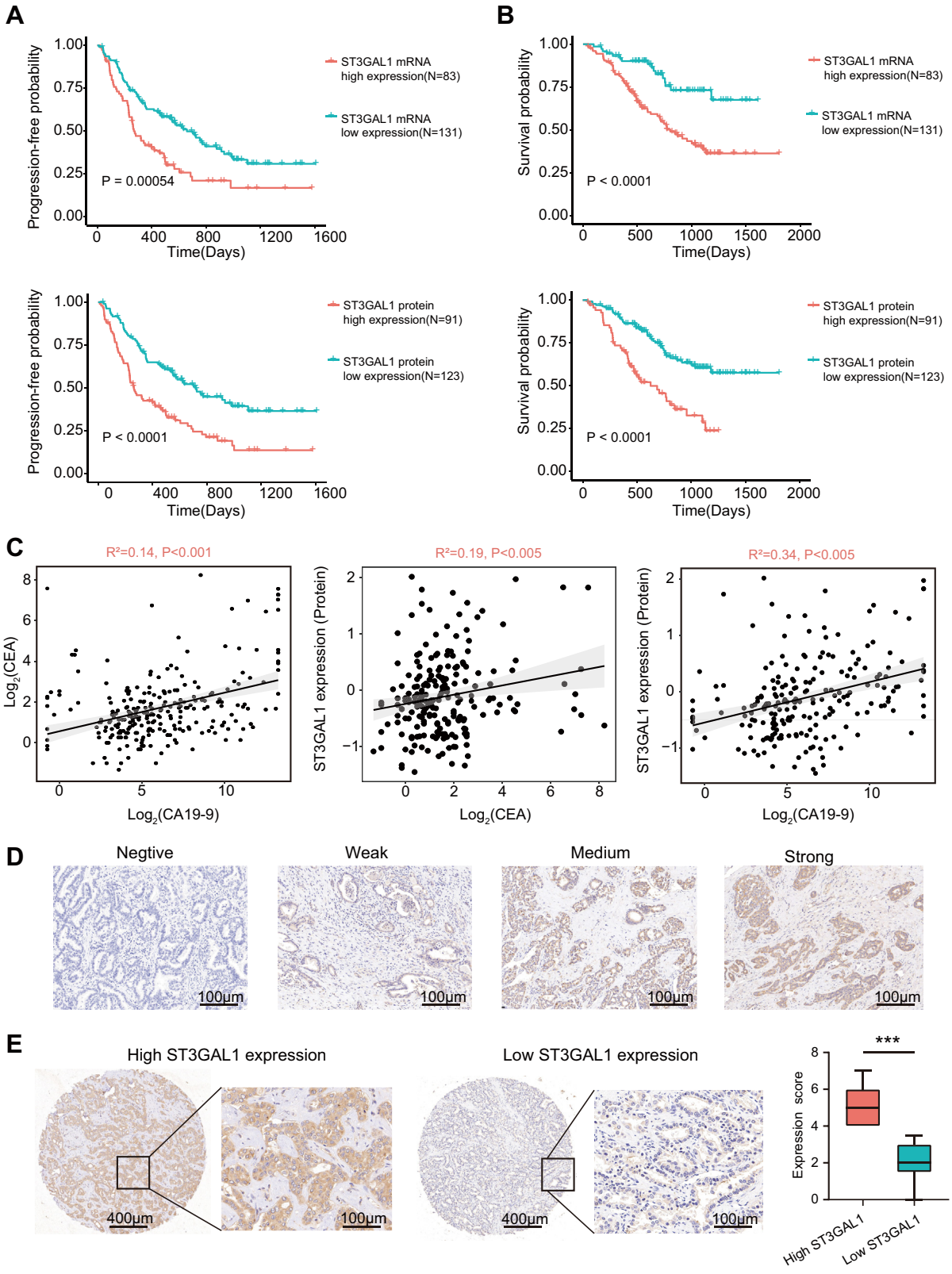

FIG. 1. **Clinical importance of ST3GAL1 in iCCA**. *A* and *B*, high and low expression refers to the expression level of ST3GAL1 in the cohort of 262 patients with iCCA. The results of Kaplan Meier survival analyses showed that patients with high expression of ST3GAL1 mRNA and protein suffer shorter overall survival and progression-free survival. *C*, the expression level of CEA in iCCA positively correlates with the expression level

TABLE 1
Univariate and multivariate analysis of ST3GAL1 in OS of 196 patients with iCCA

Variables		Univariate analysis			Multivariate analysis		
		HR	95% CI	*p*-value	HR	95% CI	*p*-value
Age, year	< 50 *versus* ≥50	1.30	0.67–2.5	0.450	NA		
Gender	Male *versus* Female	0.96	0.62–1.5	0.840	NA		
HBsAg	Positive *versus* Negative	0.60	0.35–1.0	0.062	NA		
Tumor size (cm)	< 5 *versus* ≥5	1.70	1.1–2.7	0.020	0.97	0.59–1.58	0.891
Tumor differentiation	I-II *versus* III-IV	3.60	2.3–5.6	0.000	1.80	0.92–3.44	0.089
Lymphatic metastasis	Yes *versus* No	4.40	2.8–6.9	0.000	1.95	1.98–3.50	0.058
CEA (U/ml)	< 35 *versus* ≥35	5.80	2.8–12.0	0.000	2.50	1.13–5.66	0.024
CA19–9 (ng/ml)	< 37 *versus* ≥37	1.60	1.1–2.6	0.028	1.67	1.06–2.63	0.025
AFP (ng/ml)	< 9 *versus* ≥9	1.10	0.58–2.0	0.820	NA		

Univariate and multivariate analysis, Cox proportional hazards regression model. CI, confidence interval; HR, hazard ratio; NA, not applicable; OS, overall survival.

(Supplemental Fig. S3, *D* and *E*). It indicated that NF-κB activation was involved in ST3GAL1-mediated regulation of iCCA malignancies.

Altered O-Glycosylation in Over-expressing ST3GAL1 Cells

To comprehensively analyze the glycoproteomic profile of HCCC-9810 Vector and OE cells, we performed ZIC-HILIC-based O-glycopeptide enrichment and Nano-HPLC-MS/MS (Fig. 5*A*). In addition, we utilized MAL-I and MAL-II lectins, known for their binding affinity towards α2,3-sialylated glycan (26) in iCCA cells and the results displayed an increase in sialylation levels in HCCC-9810 OE cells (Fig. 5*B*). To explore the O-glycopeptide changes in HCCC-9810 OE cells and Vector groups, comparative analyses of O-glycoproteome and proteome were conducted and normalization of O-glycopeptide abundance by the corresponding protein abundance has been performed (Supplemental Table S5 and Fig. 5*C*). Especially, PODXL, associated with cancer cell metastatic seeding (27), was detected in HCCC-9810 OE cells with upregulated sialylated O-glycopeptides. Unsupervised hierarchical clustering analysis showed that 8 O-glycopeptides provided an O-glycosylation signature for distinguishing HCCC-9810 OE cells from the controls (Fig. 5*D*).

miR-320b Targeted ST3GAL1 and Inhibited ST3GAL1 Expression

Using publicly available databases such as miRanda, microT, miRmap, and PITA, three microRNAs were identified as potential upstream regulators of ST3GAL1 (Fig. 6*A*). The miR-320a, miR-320b, and miR-320c are members of the miR-320 family, which is downregulated during tumorigenesis and serves as a crucial suppressor of EMT, tumor proliferation, and metastasis (28). Among these, miR-320b was chosen for further investigation due to its strong negative correlation with ST3GAL1 expression based on the TCGA-cholangiocarcinoma (CHOL) dataset (Fig. 6*B*). Subsequently, qRT-PCR and Western blot analysis demonstrated that miR-320b mimics reduced the expression levels of ST3GAL1 while inhibiting miR-320b with a specific inhibitor resulted in increased ST3GAL1 expression (Fig. 6, *C* and *D*). Additionally, the TargetScan database predicted a potential binding site for miR-320b in the 3′UTR of ST3GAL1. Dual luciferase reporter assays validated that overexpression of miR-320b significantly inhibited reporter activity from the ST3GAL1 3′UTR, but not from the mutant (MUT) 3′UTR (Fig. 6*E*). Moreover, functional assays including CCK-8 and colony formation assays indicated that up-regulation of miR-320b reduced the proliferation of iCCA cells, while silencing miR-320b enhanced the proliferation ability (Fig. 6, *F* and *G*). Furthermore, transwell assays revealed that over-expression of miR-320b substantially suppressed the migration and invasion of iCCA cells (Fig. 6, *H* and *I*). These findings revealed that miR-320b played a key role in negatively regulating the malignant behaviors of iCCA cells by targeting ST3GAL1.

DISCUSSION

iCCA is known for its high mortality rates and tendency to metastasize. Glycosylation is a critical process that involves attaching sugar molecules to proteins, lipids, or other molecules, and it plays a vital role in various cellular functions such as cell-cell interactions, signaling pathways, and immune responses (29). Dysregulation of glycosylation has been implicated in cancer development and metastasis. In particular, alterations in sialylation patterns, which can be attributed to disturbances in the expression levels of sialyltransferases, have been identified as a characteristic of cancer. Research has shown that changes in sialyltransferase activity levels can influence cancer invasion and

of CA19-9. The expression of ST3GAL1 protein was also positively correlated with two commonly used serum tumor markers in iCCA. *D* and *E*, immunohistochemistry was applied to microarrays, and representative microscopic views of iCCA tissues with different levels of expression were displayed.

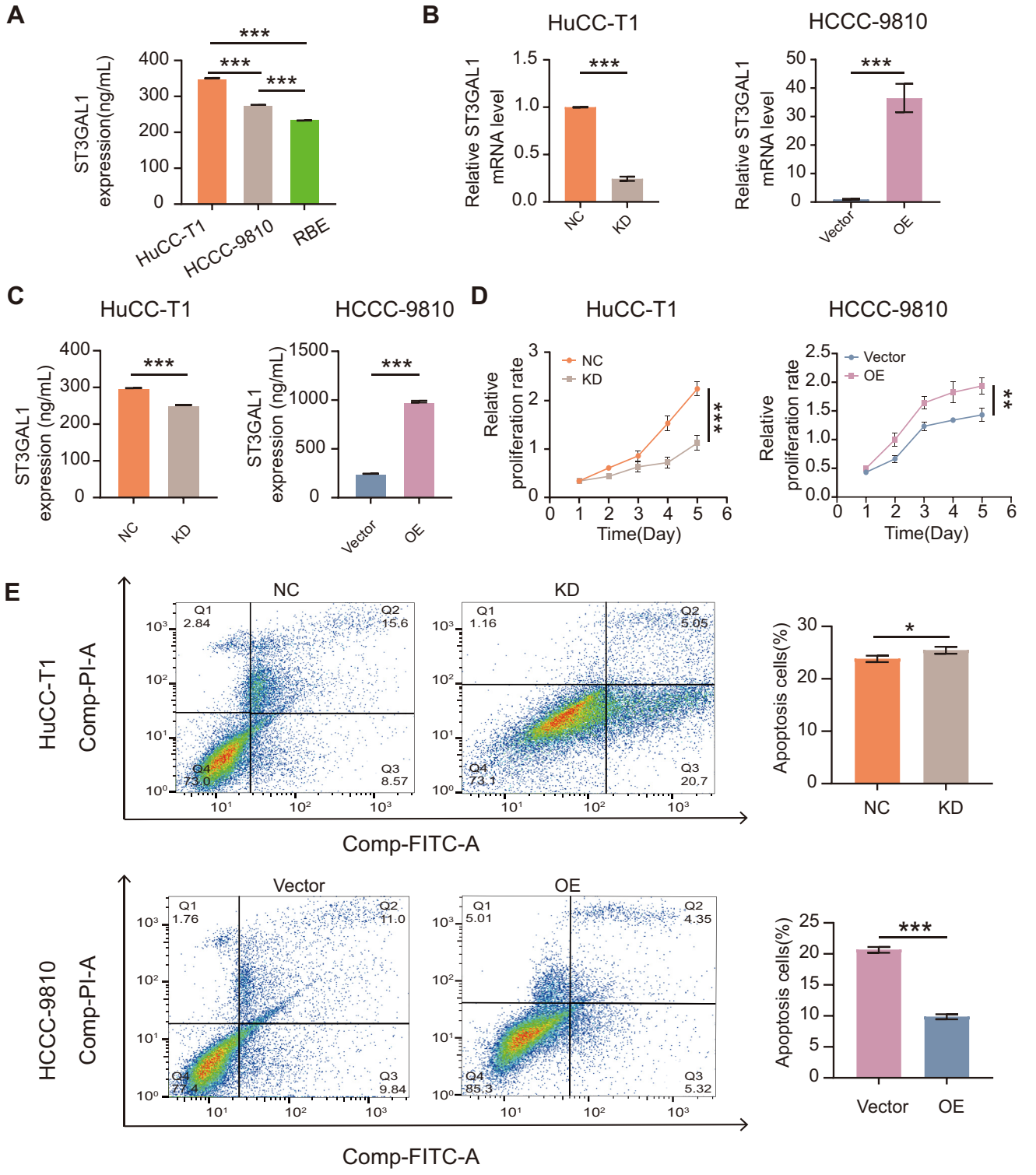

FIG. 2. **Overexpression of ST3GAL1 promoted iCCA cell proliferation and suppressed cell apoptosis**. *A*, the expression of ST3GAL1 in three iCCA cell lines (HuCC-T1, HCCC-9810, RBE) was detected by ELISA assay. *B* and *C*, the qRT-PCR, and ELISA results showed that ST3GAL1 was knocked down in HuCC-T1 and overexpressed in HCCC-9810 successfully. *D*, the proliferation ability of iCCA cells was suppressed/promoted in HuCC-T1 KD/HCCC-9810 OE cells. *E*, the cell apoptosis rate was significantly increased in HuCC-T1 KD and decreased in HCCC-9810 OE cells. $^{*}p < 0.05$, $^{**}p < 0.01$, $^{***}p < 0.001$.

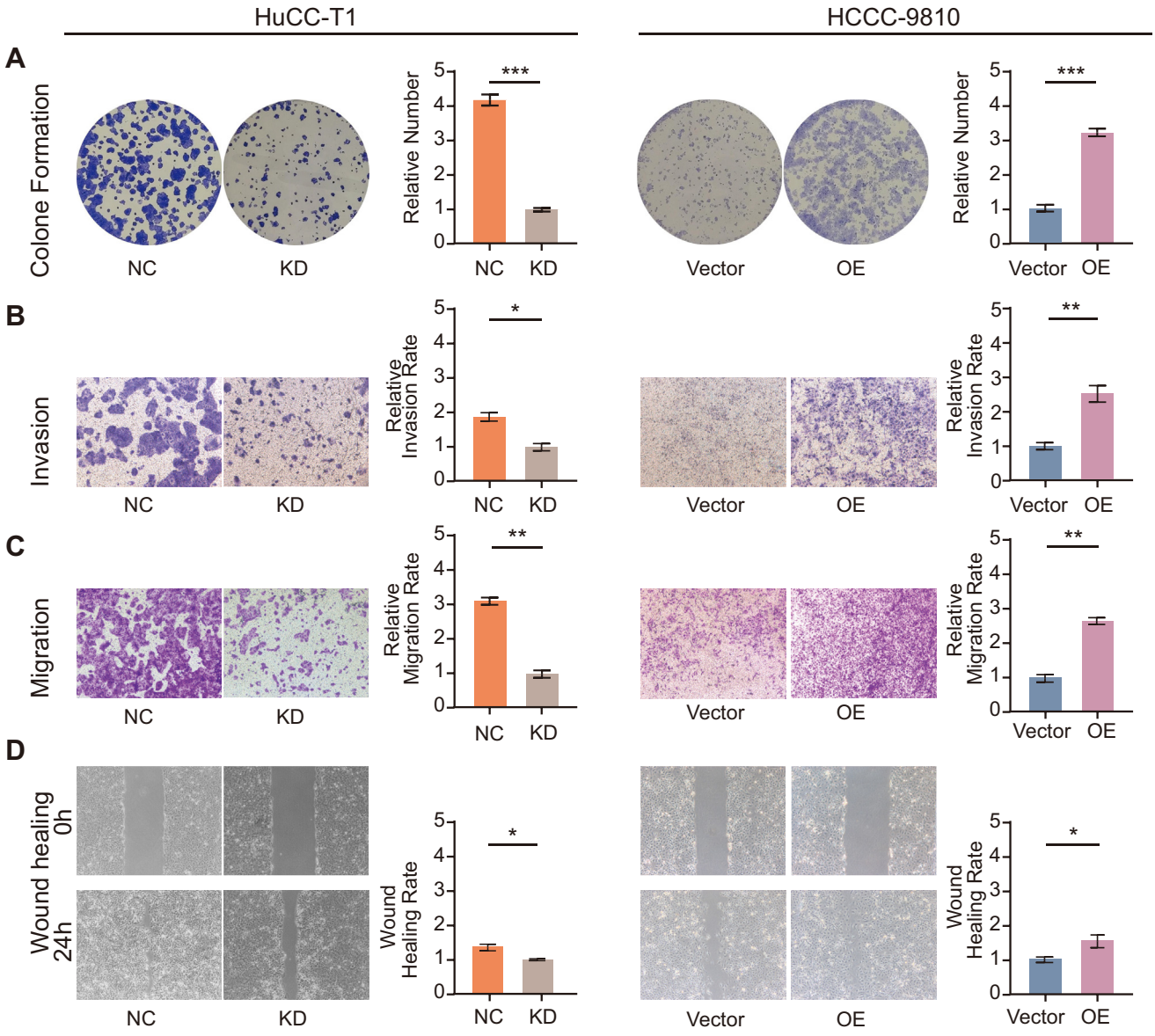

FIG. 3. **High ST3GAL1 levels increased the proliferation, invasion, and migration of iCCA cells**. *A*, the results of cell colony-forming experiments showed a weaker/stronger colony-formation ability in HuCC-T1 KD/HCCC-9810 OE cells. *B* and *C*, the transwell experiment revealed that the invasion and migration abilities of iCCA cells were suppressed/promoted in HuCC-T1 KD/HCCC-9810 OE cells. *D*, HuCC-T1 KD cell exhibited a weaker migration ability while HCCC-9810 OE cell exhibited stronger migration ability in wound healing assay. $^{*}p < 0.05$, $^{**}p < 0.01$, $^{***}p < 0.001$.

metastasis (30). For instance, studies conducted both *in vivo* and *in vitro* have demonstrated that ST3GAL1 promoted melanoma metastasis (31) and regulated stemness features essential for glioblastoma growth (32). ST3GAL1 conferred resistance to paclitaxel in ovarian cancer and promoted cell invasion and migration, indicating its potential involvement in multiple biological processes (33). Additionally, it was reported that high ST3GAL1 affected the ceramide metabolism pathway and was associated with poor prognosis in patients with osteosarcoma (34), which provided a broader perspective on the impact of ST3GAL1 on cellular function. In this study, we noted an upregulation in corrected O-glycopeptides abundances of ERP44, which may be involved in metabolic pathways altered by ST3GAL1 upregulation. It has been reported that the intracellular cysteine in ERP44 mediated a novel pathway of oxidative sensitivity and binding to RyR2. This protein-protein interaction could potentially have a significant impact on the intracellular redox environment, specifically in regulating the functions of ERP44 and RyR2, as well as cellular metabolic processes (35).

In our current study, we analyzed proteogenomic data from a cohort of 262 patients with iCCA and found that ST3GAL1, a

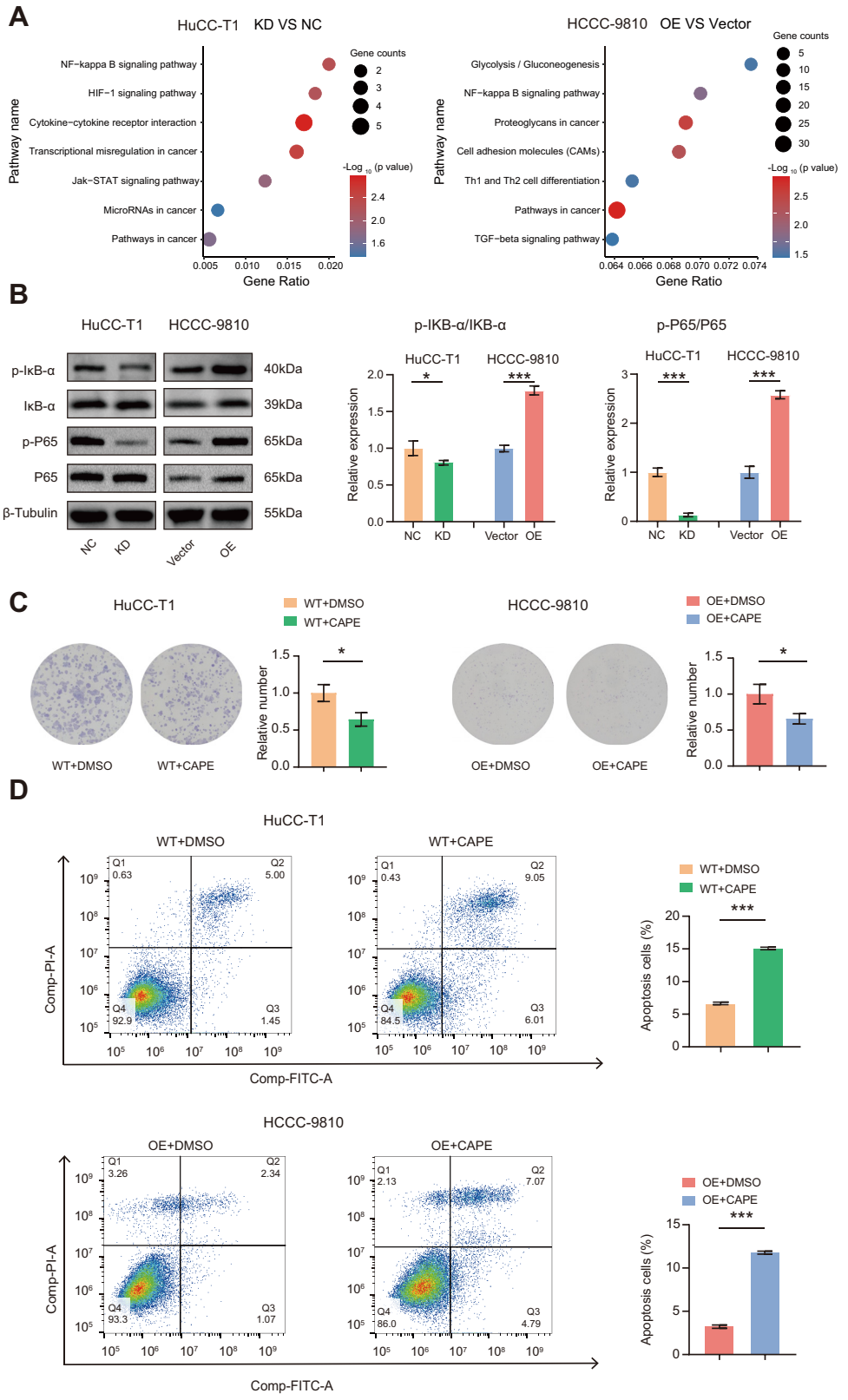

FIG. 4. **ST3GAL1 regulated proliferation *via* activating the NF-κB signaling pathway in iCCA cells**. *A*, the KEGG pathway enrichment analysis results showed the NF-κB signaling pathway was affected when ST3GAL1 was knocked down/overexpressed. *B*, major markers of NF-κB signaling were detected using Western blot, and corresponding changes were displayed. *C*, HuCC-T1 WT and HCCC-9810 OE cells were

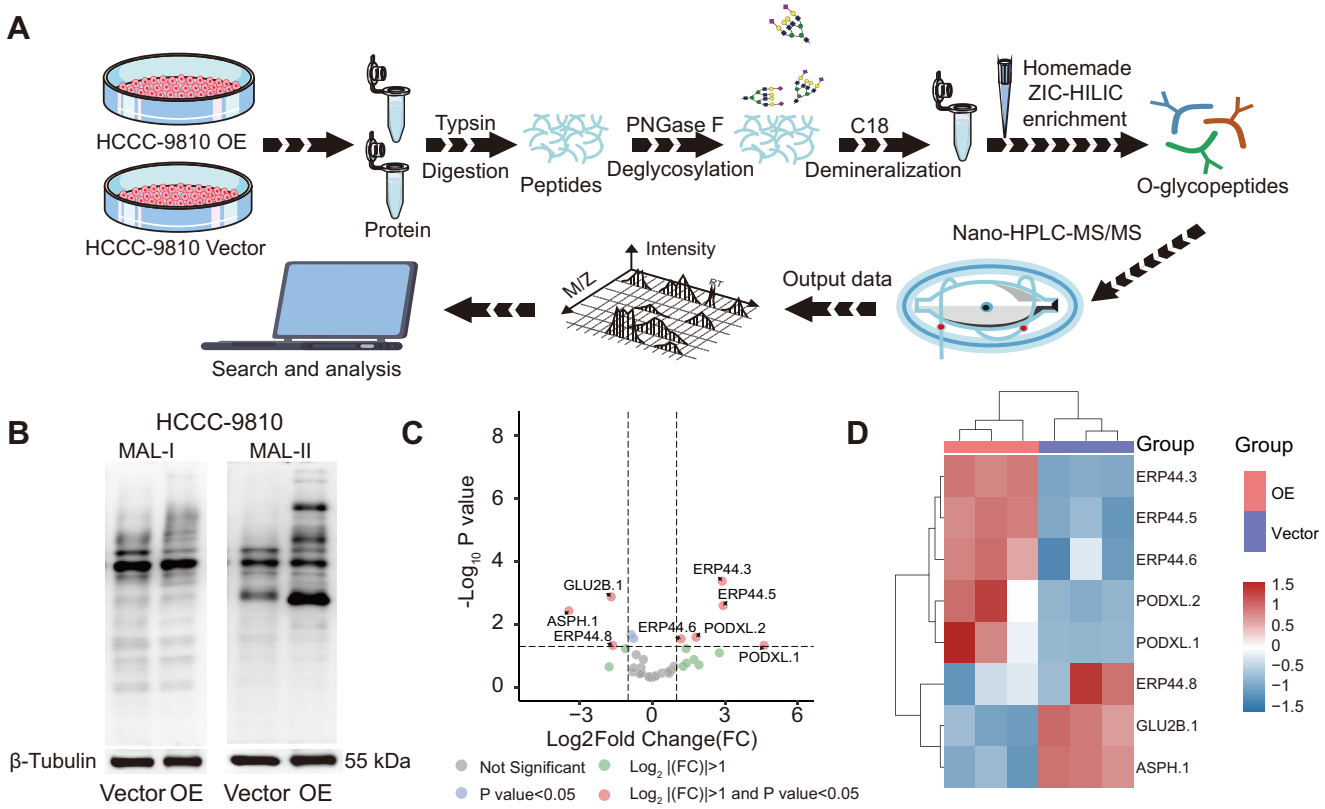

FIG. 5. **Identification of altered O-glycosylation in overexpressing ST3GAL1 cell**. *A*, the workflow of glycopeptide detection with Nano-HPLC-MS/MS. *B*, lectin blot exhibited the sialylation level when ST3GAL1 overexpression in iCCA cells. *C*, the volcano plot displayed the glycoproteins with differentially expressed O-glycopeptides between the HCCC-9810 Vector and OE cells (log_2(IFCl) >1, $p < 0.05$ after correction of O-glycopeptide abundance by protein abundance). The O-glycopeptide was indicated as a glycoprotein. number (for example, PODXL.1) and detailed peptide sequence and site-specific O-glycan composition were provided in Supplemental Table S5. *D*, the heatmap illustrated the unsupervised clustering of glycoproteins with differentially expressed O-glycopeptides. The clustering method used was complete, with Euclidean distance as the distance metric. The O-glycopeptide was indicated as a glycoprotein. number (for example, PODXL.1) and detailed peptide sequence and site-specific O-glycan composition can be accessed in Supplemental Table S5.

sialyltransferase responsible for modifying the GalNAc-O-Ser/Thr structure through α2,3 sialylation, was significantly associated with poor prognosis and adverse clinicopathological features in patients with iCCA. Consistent with previous reports of ST3GAL1 facilitating cell migration and invasion in breast cancer (36), we observed that overexpression of ST3GAL1 enhanced proliferation, migration, and invasion and inhibited apoptosis of iCCA cells *in vitro*. Importantly, using proteomic strategy, we identified that ST3GAL1 was associated with NF-κB signaling pathway, contributing to the malignancy of iCCA.

It is noteworthy that the sustained activation of NF-κB, as indicated by increased phosphorylation of P65, is a critical mechanism underlying tumorigenesis, drug resistance regulation, and tumor self-defense. For example, the NF-κB signaling pathway has been shown to contribute to the development of ovarian cancer through TRIM52 (37). In oral squamous cell carcinoma, activation of the NF-κB signaling pathway led to poor radiation response, shorter survival time (38), and decreased sensitivity to the chemotherapy drug cisplatin (39). In our study, we observed upregulation/downregulation of p-IκBα and p-P65 expressions in iCCA cells treated with synthetic ST3GLA1 lentivirus/ST3GAL1 shRNAs compared to control cells. Furthermore, the NF-κB pathway inhibitor, CAPE, not only reversed the high expression of p-P65 and p-IκBα mediated by ST3GLA1 in iCCA cells but also counteracted the effects of ST3GAL1 on iCCA cell proliferation, migration, and invasion. These results further confirmed the contribution of ST3GAL1 to the NF-κB pathway in iCCA.

As a glycosyltransferase, the function of ST3GAL1 is to regulate the phenotype of cells through modification of

cultivated with CAPE (the inhibitor of the NF-κB signaling pathway), and the colony formation ability was reversed. *D*, flow cytometry detection results showed an increased number of cell apoptosis when CAPE existed. *$p < 0.05$, ***$p < 0.001$.

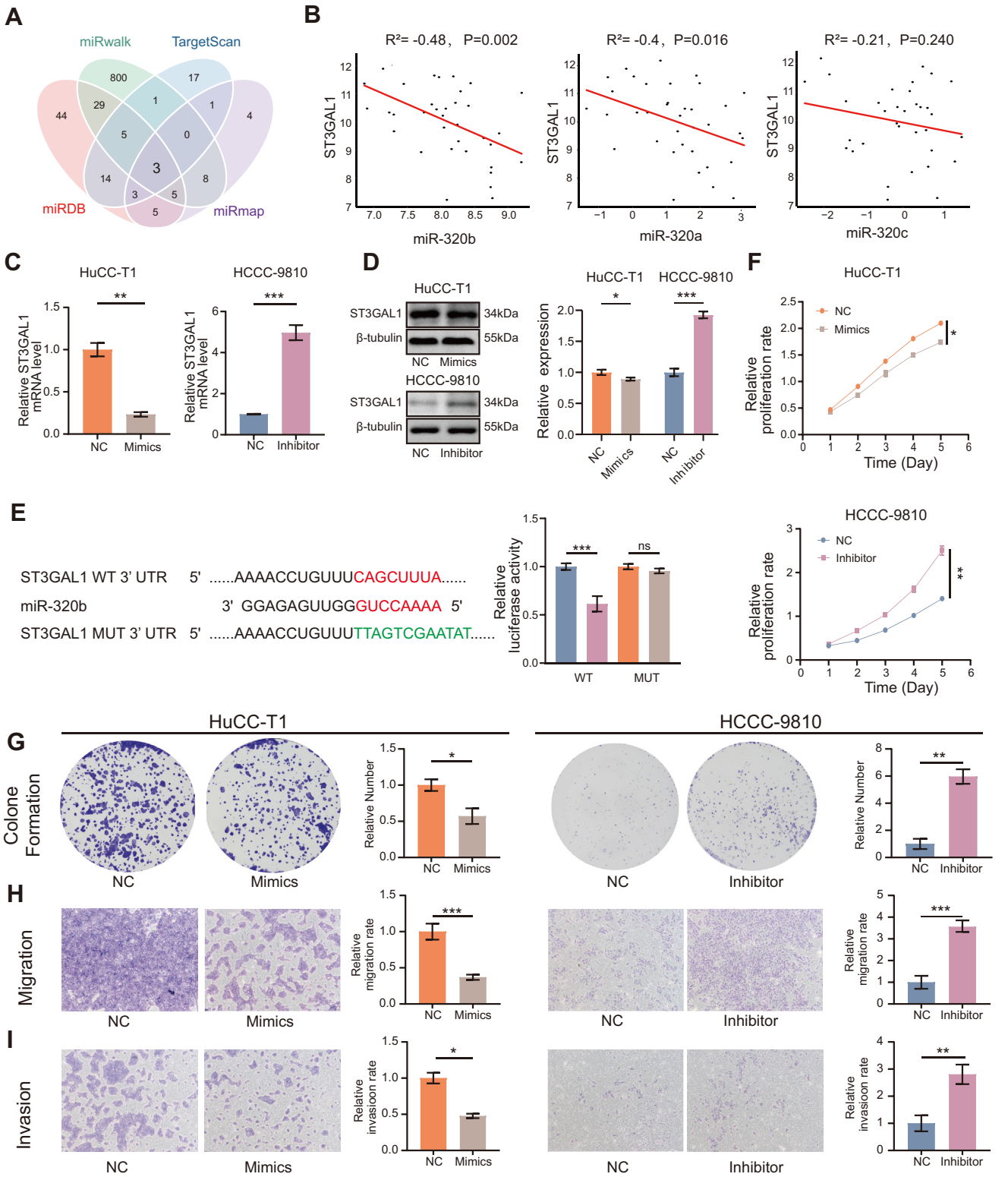

FIG. 6. **The miR-320b targeted ST3GAL1 and inhibited ST3GAL1 expression.** *A*, the miRNA binding sites of ST3GAL1 were predicted using four online databases (miRDB, miRwalk, TargetScan and miRmap) and three miRNAs were selected as candidates. *B*, correlation analyses revealed that the expression of miR-320b showed the strongest correlation with ST3GAL1. *C* and *D*, qRT-PCR and Western blot analysis of ST3GAL1 mRNA and protein expression in iCCA cells transfected with miR-320b mimics, inhibitor, or negative control. *E*, the putative miR-320b binding sequence in the 3′-UTR of ST3GAL1 was displayed. Luciferase activity of 293T cells co-transfected with ST3GAL1-3′UTR-WT or MUT

O-glycans, thereby affecting cellular behaviors. ST3GAL1 could affect cell differentiation, castration resistance, and metastasis by altering the O-glycan of CD45 and galectin-glycan interaction (40, 41). Therefore, it is crucial to discover changes in O-glycan in iCCA cells to understand the molecular mechanisms underlying ST3GAL1's functions. In this study, we revealed alterations in O-glycopeptides between HCCC-9810 OE and Vector using a glycoproteomic strategy. The O-glycoproteomic analysis displayed differential O-glycopeptides between HCCC-9810 OE cells and HCCC-9810 Vector cells. It was worth noting that, changes in different O-glycan compositions were related to cancer development and progression (29, 42). We also found that the altered O-glycopeptides in HCCC-9810 OE cells formed an O-glycosylation signature that could effectively distinguish these cells from the control group. Hierarchical clustering analysis of these glycopeptides underscored the potential utility of O-glycosylation profiling as a discriminatory marker for iCCA cells with ST3GAL1 overexpression. Sialylation, a common form of glycosylation modification, has been linked to cancer progression and metastasis. Considering the overexpression of ST3GAL1, a sialyltransferase known to influence the sialylation patterns of glycoproteins, it is crucial to evaluate whether the identified peptides exhibit sialylation. In this study, a significant upregulation of sialylated O-glycopeptide in PODXL has been observed in HCCC-9810 OE, suggesting a potential association between the sialylation status of the identified glycoprotein and iCCA progression. This protein has been reported to be an independent prognostic indicator of disease aggressiveness in several cancers (43–45). However, it is noteworthy that our investigation has not yet fully elucidated the mechanism by which ST3GLA1 influences glycopeptide alterations and subsequently impacts the functionality of iCCA. Further studies are needed to provide insights into the underlying mechanisms of ST3GAL1-mediated O-glycosylation changes and their implications for iCCA pathogenesis.

MiRNAs can regulate glycosyltransferase levels by targeting their genes. The miR-320 family, known as negative regulators of tumors, plays a crucial role in suppressing oncogenesis (28). Previous studies have also found that miR-320b, a member of the miR-320 family, was significantly downregulated in various cancers, including colorectal cancer (46) and glioblastoma (47), suggesting its involvement in tumorigenesis. Our study first evaluated the role of miR-320b in iCCA. The expression of miR-320b is negatively related to ST3GAL1 according to the TCGA-CHOL dataset. We found a negative correlation between the expression of miR-320b and ST3GAL1 based on the TCGA-CHOL dataset. Furthermore, artificially upregulating miR-320b expression significantly suppressed the proliferation, migration, and invasion of HuCC-T1 and HCCC-9810 cells, while downregulating miR-320b promoted the progression of iCCA cells.

Despite the significant findings in our study, some limitations need to be acknowledged. Although we implicated the NF-κB signaling pathway as the downstream pathway of ST3GAL1 activity, our data suggested maybe partial rescue of ST3GAL1 knockdown cells in the presence of CAPE. Besides, further study is needed to identify proteins directly glycosylated by ST3GAL1 to exert tumorigenic growth effects. Although 2D cultures are commonly used in cancer research, they do not fully mimic the *in vivo* cellular interactions and microenvironment. Previous studies have demonstrated that 3D cell culture systems better replicate phenotypic and genetic characteristics when compared with the original primary tumor (48). 3D cell culture could be used for drug screening, rapidly assessing the toxicity and efficacy of drugs on tumor cells, aiding in the discovery of new anti-cancer drugs or optimizing the therapeutic effects of existing drugs (49). In further study, the iCCA patient-derived 3D cell model is needed to establish and evaluate the potential drugs targeting ST3GAL1. Further, the unavailability of suitable control samples, including healthy liver tissues, has also posed a limitation in conducting a comprehensive molecular comparison between iCCA and normal tissue, hindering a deeper understanding of iCCA pathogenesis and progression.

In conclusion, our study provided evidence that ST3GAL1, regulated by miR-320b, played an oncogenic role in promoting cell invasion, migration, and proliferation and inhibiting apoptosis in iCCA. Moreover, our results support the activation of the NF-κB signaling pathway by ST3GAL1 overexpression and its involvement in regulating tumorigenesis in iCCA. Glycoproteomics showed that O-glycosylation was changed in iCCA cells with high ST3GAL1 expression. The altered O-glycopeptides underscored the potential utility of O-glycosylation profiling as a discriminatory marker for iCCA cells with ST3GAL1 overexpression. These findings suggested that ST3GAL1 could potentially serve as a therapeutic target for iCCA.

DATA AVAILABILITY

Datasets in this study are available at iProx (www.iprox.cn) with project ID IPX0007264000.

Supplemental Data—This article contains Supplemental data.

Funding and additional information—The work was supported by the National Key Research and Development

luciferase reporter plasmids and miR-320b mimics or negative control. *F–I*, cell lines' proliferation, colony formation, migration, and invasion abilities were measured in iCCA cells transfected with miR-320b mimics, inhibitors, or negative control. $^{*}p < 0.05$, $^{**}p < 0.01$, $^{***}p < 0.001$.

Program of China (2022YFC2505100), the Science and Technology Commission of Shanghai Municipality (20JC1418900) and National Natural Science Foundation of China (82090053).

Author contributions—F. C. writing–original draft; F. C. and K. G. formal analysis; F. C., Y. W., and Y. L. data curation; S. Z. and H. L. writing–review & editing; S. Z. project administration; S. Z. and J. S. funding acquisition; Y. L., K. G., Y. W., Y. L., Z. Y., L. D., K. G., and J. S. methodology; H. L., Q. G., and S. Z. conceptualization.

Conflicts of interest—The authors declare that they have no conflicts of interest with the contents of this article.

Abbreviations—The abbreviations used are: Annexin V-FITC, Annexin V-fluorescein isothiocyanate; ACN, Acetonitrile; AGC, Automatic gain control; CA19-9, Carbohydrate antigen 19-9; CAPE, Caffeic acid phenethyl ester; CCK-8, Cell-counting kit-8; CEA, Carcinoembryonic antigen; DEPs, Deferentially expressed proteins; FA, Formic acid; FBS, Fetal bovine serum; FC, Fold change; FDR, False discovery rates; FPKM, Fragments per kilobase per million read; IAA, Iodoacetamide; iCCA, Intrahepatic cholangiocarcinoma; IT, Injection time; DTT, Dithiothreitol; KEGG, Kyoto encyclopedia of genes and genomes; MAL-I, *Maackia amurensis* lectin I; MAL-II, *Maackia amurensis* lectin II; miRNAs, MicroRNAs; NC, Negative control; NEUs, Neuraminidases; Nano-HPLC-MS/MS, Nano high performance liquid chromatography tandem mass spectrometry; OS, Overall survival; PFS, Progression-free survival; PI, Propidium-iodide; qRT-PCR, Quantitative reverse transcription polymerase chain reaction; sh-RNA, Short-hairpin RNA; ST3GAL1, Beta-galactoside alpha-2,3-sialyltransferase 1; STs, Sialyltransferases; TCGA-CHOL, TCGA-cholangiocarcinoma; TFA, Trifluoroacetic acid; TMA, Tissue microarray; WT, Wild type; XIC, extracted-ion chromatograms; ZIC-HILIC, Zwitterionic chromatography-hydrophilic interaction chromatography.

Received October 22, 2023, and in revised form, July 14, 2024
Published, MCPRO Papers in Press, July 26, 2024, https://doi.org/10.1016/j.mcpro.2024.100821

REFERENCES

1. Valle, J. W., Lamarca, A., Goyal, L., Barriuso, J., and Zhu, A. X. (2017) New horizons for precision medicine in biliary tract cancers. *Cancer Discov.* **7**, 943–962
2. Rizvi, S., Khan, S. A., Hallemeier, C. L., Kelley, R. K., and Gores, G. J. (2018) Cholangiocarcinoma - evolving concepts and therapeutic strategies. *Nat. Rev. Clin. Oncol.* **15**, 95–111
3. Moris, D., Palta, M., Kim, C., Allen, P. J., Morse, M. A., and Lidsky, M. E. (2023) Advances in the treatment of intrahepatic cholangiocarcinoma: an overview of the current and future therapeutic landscape for clinicians. *CA Cancer J. Clin.* **73**, 198–222
4. Mereiter, S., Balmana, M., Campos, D., Gomes, J., and Reis, C. A. (2019) Glycosylation in the Era of cancer-targeted therapy: where are we heading? *Cancer Cell* **36**, 6–16
5. Pinho, S. S., and Reis, C. A. (2015) Glycosylation in cancer: mechanisms and clinical implications. *Nat. Rev. Cancer* **15**, 540–555
6. Stowell, S. R., Ju, T., and Cummings, R. D. (2015) Protein glycosylation in cancer. *Annu. Rev. Pathol.* **10**, 473–510
7. Magalhaes, A., Duarte, H. O., and Reis, C. A. (2021) The role of O-glycosylation in human disease. *Mol. Aspects Med.* **79**, 100964
8. Scupakova, K., Adelaja, O. T., Balluff, B., Ayyappan, V., Tressler, C. M., Jenkinson, N. M., *et al*. (2021) Clinical importance of high-mannose, fucosylated, and complex N-glycans in breast cancer metastasis. *JCI Insight* **6**, e146945
9. Li, F., and Ding, J. (2019) Sialylation is involved in cell fate decision during development, reprogramming and cancer progression. *Protein Cell* **10**, 550–565
10. Hugonnet, M., Singh, P., Haas, Q., and von Gunten, S. (2021) The distinct roles of sialyltransferases in cancer biology and onco-immunology. *Front. Immunol.* **12**, 799861
11. Zhuo, Y., Chammas, R., and Bellis, S. L. (2008) Sialylation of beta1 integrins blocks cell adhesion to galectin-3 and protects cells against galectin-3-induced apoptosis. *J. Biol. Chem.* **283**, 22177–22185
12. Tajadura-Ortega, V., Gambardella, G., Skinner, A., Halim, A., Van Coillie, J., Schjoldager, K. T. G., *et al*. (2021) O-linked mucin-type glycosylation regulates the transcriptional programme downstream of EGFR. *Glycobiology* **31**, 200–210
13. Laubli, H., Kawanishi, K., George Vazhappilly, C., Matar, R., Merheb, M., and Sarwar Siddiqui, S. (2021) Tools to study and target the Siglec-sialic acid axis in cancer. *FEBS J.* **288**, 6206–6225
14. Schmiedel, J. M., Klemm, S. L., Zheng, Y., Sahay, A., Bluthgen, N., Marks, D. S., *et al*. (2015) Gene expression. MicroRNA control of protein expression noise. *Science* **348**, 128–132
15. Neelamegham, S., and Mahal, L. K. (2016) Multi-level regulation of cellular glycosylation: from genes to transcript to enzyme to structure. *Curr. Opin. Struct. Biol.* **40**, 145–152
16. Agrawal, P., Kurcon, T., Pilobello, K. T., Rakus, J. F., Koppolu, S., Liu, Z., *et al*. (2014) Mapping posttranscriptional regulation of the human glycome uncovers microRNA defining the glycocode. *Proc. Natl. Acad. Sci. U. S. A.* **111**, 4338–4343
17. Gaziel-Sovran, A., Segura, M. F., Di Micco, R., Collins, M. K., Hanniford, D., Vega-Saenz de Miera, E., *et al*. (2011) miR-30b/30d regulation of GalNAc transferases enhances invasion and immunosuppression during metastasis. *Cancer Cell* **20**, 104–118
18. Dong, L., Lu, D., Chen, R., Lin, Y., Zhu, H., Zhang, Z., *et al*. (2022) Proteogenomic characterization identifies clinically relevant subgroups of intrahepatic cholangiocarcinoma. *Cancer Cell* **40**, 70–87.e15
19. Chen, F., Li, Y., Aye, L., Wu, Y., Dong, L., Yang, Z., *et al*. (2023) FUT8 is regulated by miR-122-5p and promotes malignancies in intrahepatic cholangiocarcinoma *via* PI3K/AKT signaling. *Cell Oncol. (Dordr)* **46**, 79–91
20. Mortazavi, A., Williams, B. A., McCue, K., Schaeffer, L., and Wold, B. (2008) Mapping and quantifying mammalian transcriptomes by RNA-Seq. *Nat. Methods* **5**, 621–628
21. Roushan, A., Wilson, G. M., Kletter, D., Sen, K. I., Tang, W., Kil, Y. J., *et al*. (2021) Peak filtering, peak annotation, and wildcard search for glycoproteomics. *Mol. Cell Proteomics* **20**, 100011
22. Wang, Q., Wang, T., Wu, W. W., Lin, C. Y., Yang, S., Yang, G., *et al*. (2022) Comprehensive N- and O-glycoproteomic analysis of multiple Chinese hamster ovary host cell lines. *J. Proteome Res.* **21**, 2341–2355
23. Izquierdo-Sanchez, L., Lamarca, A., La Casta, A., Buettner, S., Utpatel, K., Klumpen, H. J., *et al*. (2022) Cholangiocarcinoma landscape in Europe: diagnostic, prognostic and therapeutic insights from the ENSCCA Registry. *J. Hepatol.* **76**, 1109–1121
24. Viatour, P., Merville, M. P., Bours, V., and Chariot, A. (2005) Phosphorylation of NF-kappaB and IkappaB proteins: implications in cancer and inflammation. *Trends Biochem. Sci.* **30**, 43–52
25. Stahli, A., Maheen, C. U., Strauss, F. J., Eick, S., Sculean, A., and Gruber, R. (2019) Caffeic acid phenethyl ester protects against oxidative stress and dampens inflammation *via* heme oxygenase 1. *Int. J. Oral Sci.* **11**, 6
26. Geisler, C., and Jarvis, D. L. (2011) Effective glycoanalysis with Maackia amurensis lectins requires a clear understanding of their binding specificities. *Glycobiology.* **21**, 988–993
27. Dashzeveg, N. K., Jia, Y., Zhang, Y., Gerratana, L., Patel, P., Shajahan, A., *et al*. (2023) Dynamic glycoprotein hyposialylation promotes chemotherapy evasion and metastatic seeding of quiescent circulating tumor cell clusters in breast cancer. *Cancer Discov.* **13**, 2050–2071

28. Liang, Y., Li, S., and Tang, L. (2021) MicroRNA 320, an anti-oncogene target miRNA for cancer therapy. *Biomedicines* **9**, 591
29. Oliveira-Ferrer, L., Legler, K., and Milde-Langosch, K. (2017) Role of protein glycosylation in cancer metastasis. *Semin. Cancer Biol.* **44**, 141–152
30. Cui, H., Lin, Y., Yue, L., Zhao, X., and Liu, J. (2011) Differential expression of the alpha2,3-sialic acid residues in breast cancer is associated with metastatic potential. *Oncol. Rep.* **25**, 1365–1371
31. Pietrobono, S., Anichini, G., Sala, C., Manetti, F., Almada, L. L., Pepe, S., *et al*. (2020) ST3GAL1 is a target of the SOX2-GLI1 transcriptional complex and promotes melanoma metastasis through AXL. *Nat. Commun.* **11**, 5865
32. Chong, Y. K., Sandanaraj, E., Koh, L. W., Thangaveloo, M., Tan, M. S., Koh, G. R., *et al*. (2016) ST3GAL1-Associated transcriptomic Program in glioblastoma tumor growth, invasion, and prognosis. *J. Natl. Cancer Inst.* **108**, djv326
33. Wu, X., Zhao, J., Ruan, Y., Sun, L., Xu, C., and Jiang, H. (2018) Sialyltransferase ST3GAL1 promotes cell migration, invasion, and TGF-beta1-induced EMT and confers paclitaxel resistance in ovarian cancer. *Cell Death Dis.* **9**, 1102
34. Zou, Y., Guo, S., Liao, Y., Chen, W., Chen, Z., Chen, J., *et al*. (2024) Ceramide metabolism-related prognostic signature and immunosuppressive function of ST3GAL1 in osteosarcoma. *Transl. Oncol.* **40**, 101840
35. Hamilton, S., Terentyeva, R., Bogdanov, V., Kim, T. Y., Perger, F., Yan, J., *et al*. (2022) Ero1alpha-Dependent ERp44 dissociation from RyR2 contributes to cardiac arrhythmia. *Circ. Res.* **130**, 711–724
36. Yeo, H. L., Fan, T. C., Lin, R. J., Yu, J. C., Liao, G. S., Chen, E. S., *et al*. (2019) Sialylation of vasorin by ST3Gal1 facilitates TGF-beta1-mediated tumor angiogenesis and progression. *Int. J. Cancer* **144**, 1996–2007
37. Yang, W., Liu, L., Li, C., Luo, N., Chen, R., Li, L., *et al*. (2018) TRIM52 plays an oncogenic role in ovarian cancer associated with NF-kB pathway. *Cell Death Dis.* **9**, 908
38. Bhat, K. P. L., Balasubramaniyan, V., Vaillant, B., Ezhilarasan, R., Hummelink, K., Hollingsworth, F., *et al*. (2013) Mesenchymal differentiation mediated by NF-kappaB promotes radiation resistance in glioblastoma. *Cancer Cell* **24**, 331–346
39. Huang, Z., Zhang, Y., Li, H., Zhou, Y., Zhang, Q., Chen, R., *et al*. (2019) Vitamin D promotes the cisplatin sensitivity of oral squamous cell carcinoma by inhibiting LCN2-modulated NF-kappaB pathway activation through RPS3. *Cell Death Dis.* **10**, 936
40. Giovannone, N., Antonopoulos, A., Liang, J., Geddes Sweeney, J., Kudelka, M. R., King, S. L., *et al*. (2018) Human B cell differentiation is characterized by progressive remodeling of O-linked glycans. *Front. Immunol.* **9**, 2857
41. Tzeng, S. F., Tsai, C. H., Chao, T. K., Chou, Y. C., Yang, Y. C., Tsai, M. H., *et al*. (2018) O-Glycosylation-mediated signaling circuit drives metastatic castration-resistant prostate cancer. *FASEB J.* **15**, fj201800687
42. Nielsen, M. I., de Haan, N., Kightlinger, W., Ye, Z., Dabelsteen, S., Li, M., *et al*. (2022) Global mapping of GalNAc-T isoform-specificities and O-glycosylation site-occupancy in a tissue-forming human cell line. *Nat. Commun.* **13**, 6257
43. Boman, K., Larsson, A. H., Segersten, U., Kuteeva, E., Johannesson, H., Nodin, B., *et al*. (2013) Membranous expression of podocalyxin-like protein is an independent factor of poor prognosis in urothelial bladder cancer. *Br. J. Cancer* **108**, 2321–2328
44. Lin, C. W., Sun, M. S., and Wu, H. C. (2014) Podocalyxin-like 1 is associated with tumor aggressiveness and metastatic gene expression in human oral squamous cell carcinoma. *Int. J. Oncol.* **45**, 710–718
45. Roman-Fernandez, A., Mansour, M. A., Kugeratski, F. G., Anand, J., Sandilands, E., Galbraith, L., *et al*. (2023) Spatial regulation of the glycocalyx component podocalyxin is a switch for prometastatic function. *Sci. Adv.* **9**, eabq1858
46. Dong, Y., Wu, W. K., Wu, C. W., Sung, J. J., Yu, J., and Ng, S. S. (2011) MicroRNA dysregulation in colorectal cancer: a clinical perspective. *Br. J. Cancer* **104**, 893–898
47. Tang, W., Wang, D., Shao, L., Liu, X., Zheng, J., Xue, Y., *et al*. (2020) LINC00680 and TTN-AS1 stabilized by EIF4A3 promoted malignant biological behaviors of glioblastoma cells. *Mol. Ther. Nucleic Acids* **19**, 905–921
48. Rauth, S., Karmakar, S., Batra, S. K., and Ponnusamy, M. P. (2021) Recent advances in organoid development and applications in disease modeling. *Biochim. Biophys. Acta Rev. Cancer* **1875**, 188527
49. Veninga, V., and Voest, E. E. (2021) Tumor organoids: opportunities and challenges to guide precision medicine. *Cancer Cell* **39**, 1190–1201